Reference 42

Laterally Coupled Buried Heterostructure High-Q Ring Resonators

Seung June Choi, *Member, IEEE*, Kostadin Djordjev, Zhen Peng, Qi Yang, Sang Jun Choi, and P. Daniel Dapkus, *Fellow, IEEE*

***Abstract*—All-buried InP–InGaAsP ring resonators laterally coupled to bus waveguides are demonstrated. The buried configurations offer a lower built-in refractive index step along the resonator periphery, which affords enhanced optical coupling coefficients between the waveguides and reduced scattering losses caused by the resonator sidewall imperfections. Very low optical intensity attenuations of 0.4 cm^{-1} and coupling-limited quality factors of greater than 10^5 are observed from 200-μm-radii ring resonators. The measured spectral linewidth is as narrow as 0.0145 nm.**

***Index Terms*—Buried heterostructure, epitaxial regrowth, quality (Q) factors, ring resonator.**

I. Introduction

BUS-COUPLED optical microring resonators are versatile components for wavelength filtering, multiplexing, switching, and modulating in photonic integrated circuits [1]. In these applications, the bandwidth of the resonator must be matched to the signal source to minimize signal distortion. There are other applications such as optical signal processing, spectroscopy, and laser cavity stabilization in which very narrow linewidths are required [2]. Achieving narrow linewidth filters in resonators fabricated from high index materials, such as semiconductors, has been problematic owing to the strength of surface scattering loss $\alpha_{\rm scat}$ for whispering gallery modes (WGMs). These losses along with free carrier losses $\alpha_{\rm fc}$ and waveguide coupling (characterized by the coupling coefficient κ) have limited the Q of semiconductor WGM resonators to less than 2.0×10^4.

In this letter, we present a technology to realize very high Qs in semiconductor ring resonators laterally coupled to input–output (I/O) bus waveguides. For laterally coupled designs, air-guided rib type waveguides have been widely used where the air cladding affords strong mode confinement in the lateral direction to avoid radiative bending losses ($\alpha_{\rm bend}$) in small-radii rings. Since the scattering loss $\alpha_{\rm scat}$ is proportional to $\Delta n^2 = n_{\rm wg}^2 - n_{\rm cl}^2$, where $n_{\rm wg}$ and $n_{\rm cl}$ are the refractive indexes of the waveguide core and the cladding materials, respectively [3], reduction of Δn^2 will reduce the scattering loss. $\alpha_{\rm scat}$'s of 5–30 cm^{-1} have been reported from small radius air-guided semiconductor ring add–drop filters [4]. Besides $\alpha_{\rm scat}$, the strong lateral mode confinement makes it difficult to attain controllable evanescent mode coupling to adjacent waveguides. Typically, submicrometer (<0.2 μm) lateral separations must be defined for acceptable κ's between the resonator and the I/O bus waveguides, which is difficult to achieve controllably in thick waveguide structures.

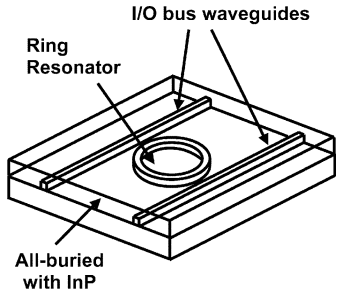

Fig. 1. Schematic drawing of an all-buried laterally coupled ring resonator.

To counter these difficulties, we propose all-buried heterostructure resonators (Fig. 1) in which the InGaAsP ($n = 3.361$) ring and bus waveguides are completely buried with InP ($n = 3.168$). The all-buried structure offers relatively weak lateral mode confinement that brings several benefits in bus-coupled microresonators. First, enhanced and controllable κ's are available through a high-index coupling medium. The physical separations between the resonator and the bus waveguides d in buried structures can be several times wider than those in air-guided devices for reasonable κ's and are realizable without using e-beam lithography. Second, considerably reduced $\alpha_{\rm scat}$ is expected from the buried waveguides due to the lowered index step. Using the buried configurations, we can realize low-loss microresonators and consequently achieve very high Qs that are controlled and limited by κ's. However, the reduced index step built into buried circular microresonators will result in significant $\alpha_{\rm bend}$ unless the radius of the resonator is made large enough [5]. We designed 200-μm radius all-buried heterostructure rings to minimize $\alpha_{\rm bend}$ as well as $\alpha_{\rm scat}$. The technology used here enables us to investigate high-Q resonant characteristics in a coupling-limited regime.

II. Design and Experiment

Using a full-vectorial mode solver, we calculate $\alpha_{\rm bend}$ for the given material systems to determine the appropriate dimensions of rings. The ring used for this calculation has 0.9×0.4 μm^2 cross-sectional area with the material indexes given in Table I. The calculation predicts that the ring radius (R) must be larger than 80 μm to maintain $\alpha_{\rm bend} < 1$ cm^{-1} and $R = 200$ μm ensures $\alpha_{\rm bend} < 0.1$ cm^{-1}. It is more difficult to assess $\alpha_{\rm scat}$, since the numerical evaluation of sidewall roughness is not straightforward. Assuming $\pm$50-nm periodic corrugations on the sidewalls and employing an index perturbation model [3],

Manuscript received March 3, 2004; revised June 1, 2004. This work was supported by Defense Advanced Research Projects Agency under the Chip-Scale Wavelength Division Multiplexing (CSWDM) Program.

The authors are with the Department of Electrical Engineering-Electrophysics, University of Southern California, Los Angeles, CA 90089 USA (e-mail: dapkus@usc.edu).

Digital Object Identifier 10.1109/LPT.2004.834518

Report Documentation Page

Form Approved
OMB No. 0704-0188

1. REPORT DATE	2. REPORT TYPE	3. DATES COVERED
01 JUN 2005	**N/A**	**-**

4. TITLE AND SUBTITLE	5a. CONTRACT NUMBER
Laterally Coupled Buried Heterostructure High-Q Ring Resonators	5b. GRANT NUMBER
	5c. PROGRAM ELEMENT NUMBER
6. AUTHOR(S)	5d. PROJECT NUMBER
	5e. TASK NUMBER
	5f. WORK UNIT NUMBER
7. PERFORMING ORGANIZATION NAME(S) AND ADDRESS(ES) **Department of Electrical Engineering-Electrophysics, University of Southern California, Los Angeles, CA 90089 USA**	8. PERFORMING ORGANIZATION REPORT NUMBER
9. SPONSORING/MONITORING AGENCY NAME(S) AND ADDRESS(ES)	10. SPONSOR/MONITOR'S ACRONYM(S)
	11. SPONSOR/MONITOR'S REPORT NUMBER(S)

12. DISTRIBUTION/AVAILABILITY STATEMENT
Approved for public release, distribution unlimited

13. SUPPLEMENTARY NOTES
See also ADM001923.

14. ABSTRACT

15. SUBJECT TERMS

16. SECURITY CLASSIFICATION OF:			17. LIMITATION OF ABSTRACT	18. NUMBER OF PAGES	19a. NAME OF RESPONSIBLE PERSON
a. REPORT	b. ABSTRACT	c. THIS PAGE			
unclassified	**unclassified**	**unclassified**	**UU**	**3**	

TABLE I
DESIGN PARAMETERS FOR THE BURIED MICRORINGS AND THE CALCULATED RADIATIVE BENDING ($\alpha_{\rm bend}$) AND SCATTERING ($\alpha_{\rm scat}$) LOSSES. PARAMETERS r, $n_{\rm wg}$, $n_{\rm cl}$, $n_{\rm eff}$, ARE THE RING RADIUS, THE REFRACTIVE INDEXES OF THE WAVEGUIDE CORE AND THE CLADDING MATERIALS, AND THE EFFECTIVE INDEX OF THE RING RESONATOR, RESPECTIVELY, FOR TRANSVERSE ELECTRIC-POLARIZATION. THE RING HAS 0.9×0.4 μm^2 CROSS-SECTIONAL AREA, AND $\pm$50-nm CORRUGATIONS ARE ASSUMED FOR THE SIDEWALL ROUGHNESS

r [μm]	n_{wg}	n_{cl}	n_{eff}	α_{bend} [cm^{-1}]	α_{scat} [cm^{-1}]
200	3.361	3.168	3.212	< 0.1	< 0.1

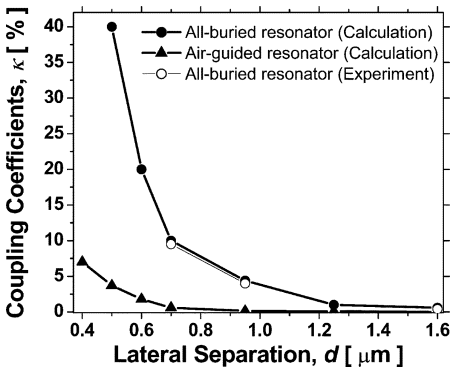

Fig. 2. Calculated and optical power coupling coefficients (κ's) versus the lateral separation (d) between the microring and the straight bus waveguide. Different lateral claddings are used for the data: air ($n = 1$, closed triangles) and InP ($n = 3.168$, closed circles), respectively. The experimental results (open circles) for $d = 0.7, 0.95,$ and 1.6 μm are also shown along with the calculated data, which proves the accuracy of the theoretical computation.

we have $\alpha_{\rm scat} < 0.1$ cm^{-1} for the given configurations. The overall design parameters are summarized in Table I.

Once the materials and physical dimensions of a ring resonator are chosen, the effective modal index ($n_{\rm eff}$) and the κ's between the ring and the bus waveguides can be computed. First, the effective index approximation is combined with a conformal transformation [7] to calculate the $n_{\rm eff}$'s of the ring and the buried bus waveguides. Then, the modal field distribution in the ring and the bus waveguides are computed by a finite difference method, from which local coupling coefficients can be calculated by solving the overlap integral of the fields and the effective index distribution. Finally, the overall κ is calculated by integrating the coupled-mode equations with respect to the propagation distance in the bus waveguides. The details can be found in [8]. Fig. 2 is instructive, comparing the calculated κ's versus the lateral separations (d's) between the ring and the bus waveguides in air-guided and buried microresonators. Here, a 200-μm-radius ring resonator having 0.9×0.4 μm^2 cross-sectional area is laterally coupled to a 0.8×0.4 μm^2 single-mode bus waveguide. The material index of the waveguide cores is 3.361 at $\lambda = 1550$ nm. Note that several times higher κ's are available for a given separation when the resonators are buried with InP. In this experiment, we have d vary from 0.7 to 1.6 μm to obtain a variation of κ from 10% to 0.5%, respectively.

To initiate the process, a 0.4-μm-thick InGaAsP ($\lambda_{\rm WG} = 1.25$ μm) waveguide layer is grown on an (001) oriented InP substrate by metal–organic chemical vapor deposition and covered by a 0.1-μm-thick SiN_x layer deposited as a masking layer. Ring and I/O bus patterns are defined and etched into this

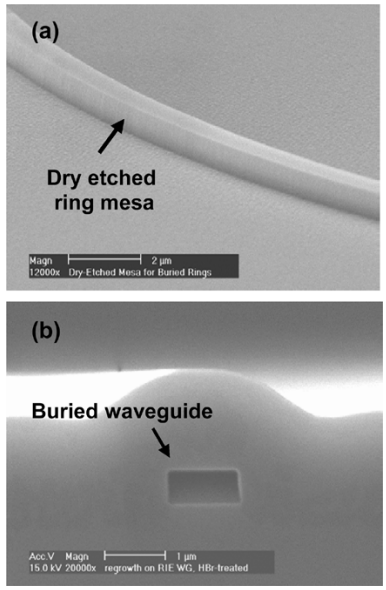

Fig. 3. (a) Scanning-electron microscopic (SEM) image of a dry-etched ring resonator mesa. (b) SEM cross-sectional view of a buried waveguide.

layer, using contact photolithography and CH_4-based reactive ion etching [9]. The straight bus lines are aligned parallel to the [110] direction. The resultant mesas are 0.8–0.9 μm wide, having smooth and vertical sidewalls as shown in Fig. 3(a). The slope of typical mesa profiles is 88°. The polymers generated on the sidewalls during the dry-etching process are cleaned by an oxygen plasma treatment and the SiN_x mask is removed by buffered oxide etchant. Finally, a 1.5-μm-thick InP layer is overgrown on the waveguide mesas to produce buried heterostructure microresonators. No voids or visible growth defects along the waveguide mesas are visible, as shown in Fig. 3(b). The wafer is mechanically thinned and cleaved for measurements, followed by antireflection (AR) coatings on the cleaved facets.

III. RESULTS AND DISCUSSIONS

The optical transmission spectra are measured from straight unloaded (i.e., not coupled to a resonator) bus waveguides before the cleaved facets are AR-coated. The optical intensity attenuation $\alpha_{\rm bus}$ can be estimated by examining the fringe oscillations of the Fabry–Pérot resonant characteristics [10]. Typically, low $\alpha_{\rm bus}$'s of 0.2–0.3 cm^{-1} are obtained from the buried straight bus waveguides. The origin of the optical losses observed in the buried straight waveguides is not clearly identified yet. The residual material losses in the nominally undoped waveguide and scattering losses may both contribute to the measured losses.

The optical resonant transmission spectra of the buried rings are then measured by coupling an external tunable laser into the AR-coated bus waveguide facet and collecting the transmitted signal at the other end of the bus line. Using the coupling of modes in time (CMT) formalism [1], the normalized transmission spectrum can be described as

$$T = \frac{j\left(\frac{\Delta\omega}{\omega_0} + \frac{\Delta n}{n_0}\right) + \frac{1}{2}\left(Q_{\rm loss}^{-1} + Q_{\rm couple\text{-}out}^{-1} - Q_{\rm couple\text{-}in}^{-1}\right)}{j\left(\frac{\Delta\omega}{\omega_0} + \frac{\Delta n}{n_0}\right) + \frac{1}{2}\left(Q_{\rm loss}^{-1} + Q_{\rm couple\text{-}out}^{-1} + Q_{\rm couple\text{-}in}^{-1}\right)} \quad (1)$$

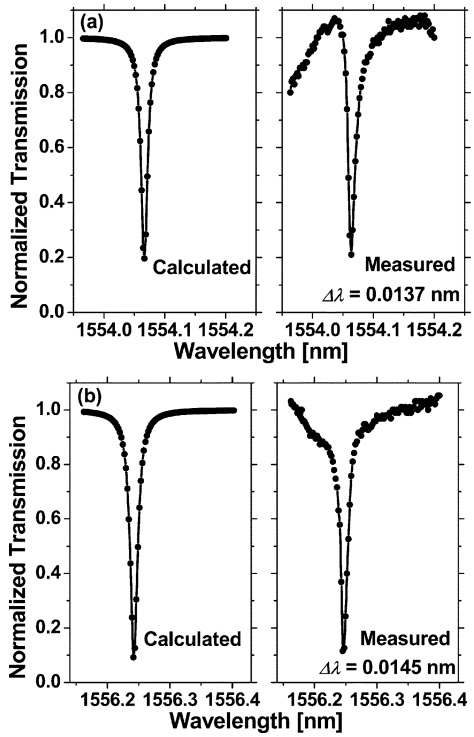

Fig. 4. Calculated (left) and the measured (right) transmission spectra of 200-μm-radii buried ring resonators. The spectral resolution is 0.0024 nm. (a) Type 1 and (b) Type 2.

where $\Delta\omega$ is the detuning from the resonance and Δn accounts for the change of resonance caused by the change of the refractive index (terms of the Δn^2 order are neglected). The associated Qs are defined as follows:

$$Q_{\text{loss}} = \omega_o \tau_{PH} = \frac{\omega_o \tau_{\text{RT}}}{L_{\text{RT}}} = \frac{\omega_o \frac{2\pi r n_{\text{eff}}}{c}}{1 - \exp[-2\pi r \alpha]}$$
$$Q_{\text{couple-in}} = \frac{4\pi^2 r n_{\text{eff}}}{\lambda_o \kappa_{\text{in}}}, \quad Q_{\text{couple-out}} = \frac{4\pi^2 r n_{\text{eff}}}{\lambda_o \kappa_{\text{out}}}. \quad (2)$$

Here, α, κ_{in}, κ_{out}, Q_{loss}, $Q_{\text{couple-in}}$, and $Q_{\text{couple-out}}$ represent the optical intensity attenuation, I/O power coupling coefficients, the Q factors associated with the loss, and the coupling coefficients, respectively. Note that $L_{\text{RT}} = 1 - \exp[-2\pi r\alpha]$ corresponds to the optical round-trip loss in the ring resonator.

Fig. 4(a) and (b) shows the measured and calculated transmission spectra $|T|^2$ for two different types of rings. Type 1 has identical d's for the I/O bus waveguides for symmetric couplings, and Type 2 is designed to be asymmetric. Equations (1) and (2) are used for the data fitting processes. Table II summarizes the experimental device parameters for Types 1 and 2, where we find that the estimated κ's and α's are quite consistent with the calculated values and the α_{bus} measured from straight bus waveguides, respectively. The experimental results of κ's for $d = 0.7, 0.95,$ and 1.6 μm are shown along with the calculated data in Fig. 2. Qs as high as 1.3×10^5 are observed in these devices. Slightly higher Qs are observed from the symmetric design due to the lower overall κ's, while superior extinctions are obtained from the asymmetric device because of the closer match to the critical coupling condition. Note that the Q of Type 2 resonator is actually limited by the $Q_{\text{couple-in}}$.

TABLE II
EXPERIMENTAL DATA DERIVED FROM CMTS FOR THE BURIED MICRORINGS IN FIG. 4. HERE, α, κ_{in}, κ_{out}, Q_{loss}, $Q_{\text{couple-in}}$, AND $Q_{\text{couple-out}}$ REPRESENT THE OPTICAL INTENSITY ATTENUATION, I/O POWER COUPLING COEFFICIENTS, THE Q FACTOR ASSOCIATED WITH THE LOSS, AND THE Q FACTORS ASSOCIATED WITH THE I/O POWER COUPLING COEFFICIENTS, RESPECTIVELY. ROW $E > 0 (E < 0)$ MEANS THAT THE RESONATOR IS OVER-COUPLED (UNDER-COUPLED)

	Parameters	Type 1 (Symmetric)	Type 2 (Asymmetric)
A	d_{in} / d_{out} [μm]	0.95 / 0.95	0.70 / 1.60
B	κ_{in} / κ_{out} [%]	4.0 / 4.0	9.5 / 0.4
C	α [cm^{-1}]	0.4	0.4
D	$L_{RT} = 1 - \exp(-2\pi r)$ [%]	4.9	4.9
E	$\kappa_{in} - (\kappa_{out} + L_{RT})$	-4.9	+4.2
F	$Q_{couple\text{-}in}$ / $Q_{couple\text{-}out}$	400000 / 400000	170000 / 4000000
G	Q_{loss}	330000	330000
H	Q	113000	107000

The measured spectral linewidths ($\Delta\lambda$s) of Types 1 and 2 are 0.0137 and 0.0145 nm, respectively. The measured free spectral ranges (FSRs) are approximately 0.54 nm for each type of device, which indicates finesse ($F = \text{FSR}/\Delta\lambda$) values of 37–39.

In conclusion, all-buried InP–InGaAsP ring resonators laterally coupled to bus waveguides are demonstrated. The suggested technology allows us to investigate optical resonant characteristics in a coupling-limited regime with Qs of 10^5 or higher. These high-Q resonators may also be suitable for optical signal processing, chip scale spectrometers, and narrow linewidth lasers.

REFERENCES

[1] B. E. Little, S. T. Chu, H. A. Haus, J. Foresi, and J. -P. Laine, "Microring resonator channel dropping filters," *J. Lightwave Technol.*, vol. 15, pp. 998–1005, June 1997.

[2] D. K. Armani, T. J. Kippenberg, S. M. Spillane, and K. J. Vahala, "Ultra-high-Q toroid microcavity on a chip," *Nature*, vol. 421, pp. 925–928, Feb. 2003.

[3] J. P. R. Lacey and F. P. Payne, "Radiation loss from planar waveguides with random wall imperfections," in *Proc. Inst. Elect. Eng.*, vol. 137, Aug. 1990, pp. 282–288.

[4] D. Rafizadeh, J. P. Zhang, R. C. Tiberio, and S. T. Ho, "Propagation loss measurements in semiconductor ring and disk resonators," *J. Lightwave Technol.*, vol. 16, pp. 1308–1314, July 1998.

[5] E. A. J. Marcatili, "Dielectric rectangular waveguide and directional coupler for integrated optics," *Bell Syst. Tech. J.*, vol. 48, pp. 2071–2102, 1969.

[6] M. K. Chin and S. T. Ho, "Design and modeling of waveguide-coupled single-mode microring resonators," *J. Lightwave Technol.*, vol. 16, pp. 1433–1446, Aug. 1998.

[7] D. R. Rowland and J. D. Love, "Evanescent wave coupling of whispering gallery modes of a dielectric cylinder," *Proc. Inst. Elect. Eng.*, vol. 140, no. 3, pp. 177–188, Mar. 1993.

[8] K. D. Djordjev, "Active microdisk resonant devices and semiconductor optical equalizers as building blocks for future photonic circuitry," Ph.D. thesis, Univ. Southern California, 2002.

[9] S. J. Choi, K. D. Djordjev, S. J. Choi, and P. D. Dapkus, "CH4-based dry etching of high Q InP microdisks," *J. Vac. Sci. Technol. B*, vol. 20, pp. 301–305, Jan. 2002.

[10] L. S. Yu, Q. Z. Liu, S. A. Pappert, P. K. L. Yu, and S. S. Lau, "Laser spectral linewidth dependence on waveguides loss measurements using the Fabry–Pérot method," *Appl. Phys. Lett.*, vol. 64, no. 5, pp. 536–538, Jan. 1994.